

A SEARCH FOR H₂O MEGAMASERS IN HIGH-Z TYPE-2 AGNS

Nicola Bennert¹

*Institute of Geophysics and Planetary Physics, University of California, Riverside, CA 92521
 bennert@physics.ucsb.edu*

Richard Barvainis²

*National Science Foundation, 4301 Wilson Boulevard, Arlington, VA 22230; and Department of Physics,
 Gettysburg College, 300 North Washington Street, Gettysburg, PA 1732
 rbarvai@nsf.gov*

Christian Henkel

*Max-Planck-Institut für Radioastronomie, Auf dem Hügel 69, D-53121 Bonn, Germany
 chenkel@mpifr-bonn.mpg.de
 and*

Robert Antonucci

*Department of Physics, University of California, Santa Barbara, CA 93106
 ski@physics.ucsb.edu*

ABSTRACT

We report a search for H₂O megamasers in 274 SDSS type-2 AGNs ($0.3 < z < 0.83$), half of which can be classified as type-2 QSOs from their [O III] 5007 luminosity, using the Robert C. Byrd Green Bank Telescope (GBT) and the Effelsberg 100-m radio telescope. Apart from the detection of the extremely luminous water vapor megamaser SDSS J080430.99+360718.1, already reported by Barvainis & Antonucci (2005), we do not find any additional line emission. This high rate of non-detections is compared to the water maser luminosity function created from the 78 water maser galaxies known to date and its extrapolation towards the higher luminosities of “gigamasers” that we would have been able to detect given the sensitivity of our survey. The properties of the known water masers are summarized and discussed with respect to the nature of high-z type-2 AGNs and megamasers in general. In the appendix, we list 173 additional objects (mainly radio galaxies, but also QSOs and galaxies) that were observed with the GBT, the Effelsberg 100-m radio telescope, or Arecibo Observatory without leading to the detection of water maser emission.

Subject headings: galaxies: active — galaxies: Seyferts — masers — quasars: general

¹Current address: Department of Physics, University of California, Santa Barbara, CA 93106

² Any opinions, findings, conclusions, and recommenda-

tions expressed in this material are those of the author and do not necessarily reflect the views of the National Science Foundation.

1. INTRODUCTION

The 22 GHz H₂O maser emission line is of great astrophysical interest for its extreme requirements for density ($>10^7 \text{ cm}^{-3}$), temperature ($>300 \text{ K}$), and of course radial velocity coherence. It is detected in both Galactic and extragalactic star forming regions as well as in the central regions of active galaxies (AGNs). In AGNs, isotropic luminosities commonly reach values of $L_{\text{H}_2\text{O}} > 10L_{\odot}$ and the objects are then classified as “megamasers” (see recent reviews by e.g. Greenhill 2004; Morganti et al. 2004; Henkel et al. 2005b; Lo 2005).

So far, water megamaser emission has been detected in about 10% of active galactic nuclei (AGNs) surveyed in the local universe (Braatz et al. 2004). The association of water megamasers with AGNs of primarily Seyfert-2 or Low-Ionization Nuclear Emission-line Region (LINER) type (Braatz et al. 1997, 2004) and the fact that the emission often arises from the innermost parsec(s) of their parent galaxy have raised great interest in the study of 22 GHz maser emission. It suggests that the so far poorly constrained excitation mechanism is closely related to AGN activity, probably irradiation by X-rays (e.g. Neufeld et al. 1994). For Seyfert-2 galaxies, in the framework of the so-called unified model (Antonucci 1993), a dusty molecular disk or torus is seen edge-on where the conditions and velocity-coherent path lengths are favorable for the formation of megamaser activity.

In those cases in which the emission arises from a nuclear disk and can be resolved spatially using Very Long Baseline Interferometry (VLBI), the central black hole (BH) mass can be constrained, as has been successfully shown for NGC 4258 (e.g. Greenhill et al. 1995; Miyoshi et al. 1995; Herrnstein et al. 1999, 2005). Moreover, using H₂O masers, distances to galaxies can be obtained without the use of standard candles (Miyoshi et al. 1995; Herrnstein et al. 1999; Argon et al. 2004; Brunthaler et al. 2005; Argon et al. 2007; Humphreys et al. 2008). Thus, finding new megamaser galaxies is of great interest.

If the unified scheme for AGNs is to be equally successful for objects of high as well as of low luminosity, there should exist a large number of type-2 QSOs whose optical spectra are dominated by

narrow emission lines. Indeed, with the advent of new extended surveys such as the Sloan Digital Sky Survey (SDSS), many type-2 QSOs have recently been identified (Zakamska et al. 2003).

We conducted a search for water megamasers in 274 of the 291 SDSS type-2 AGNs (Zakamska et al. 2003) using the Robert C. Byrd Green Bank Telescope (GBT) and the Effelsberg 100-m radio telescope. With a redshift range of $0.3 < z < 0.83$, the sample covers significantly higher distances than most previous searches for H₂O megamasers ($z \ll 0.1$; Braatz et al. 1996; Tarchi et al. 2003; Braatz et al. 2004; Kondratko et al. 2006a,b; Braatz & Gugliucci 2008; Castangia et al. 2008) and is the first survey for water megamasers in objects with QSO luminosities (except for the study of Barvainis & Antonucci (2005) which is part of the larger survey presented here).

Such a search provides clues to whether the unified model can indeed be extended to QSOs or whether their powerful engines lead to a different scenario. Do the high QSO luminosities result in H₂O “gigamasers”? Or do they destroy the warm dense molecular gas needed to supply the water molecules? Are the molecular parts of the accretion disks much farther away from the nuclear engine, so that rotation velocities are smaller in spite of a potentially more massive nuclear engine than in Seyfert-2 galaxies? Finding megamasers in type-2 QSOs may provide insights into QSO molecular disks and tori and enables us to independently determine their BH masses. Even more importantly, megamasers in type-2 QSOs may provide the unique possibility to directly measure their distances and thus verify the results from type 1a supernovae measurements on the existence and properties of the elusive dark energy (e.g. Barvainis & Antonucci 2005; Braatz et al. 2007; Reid et al. 2008).

We summarize the sample properties in §2, describe the observations in §3, present the results in §4, and discuss them in §5. After a brief summary (§6), we list a sample of 171 additional objects (radio galaxies, QSOs, and galaxies) in the Appendix (§A). Throughout the paper, we assume a Hubble constant of $H_0 = 75 \text{ km s}^{-1} \text{ Mpc}^{-1}$. For the high- z objects, we additionally assume $\Omega_\Lambda = 0.73$ and $\Omega_M = 0.27$ (Wright 2006).

2. SAMPLE PROPERTIES

As already mentioned above, our sample consists of 274 type-2 AGNs ($0.3 < z < 0.83$) selected from the SDSS (Zakamska et al. 2003). Out of these, 122 objects have $L_{[\text{OIII}]} > 3 \times 10^8 L_\odot$, and can thus be classified as type-2 QSOs (Zakamska et al. 2003). About 10% of the SDSS type-2 AGNs are radio-loud (Zakamska et al. 2004), comparable to the AGN population as a whole. A few type-2 AGNs have soft X-ray counterparts (Zakamska et al. 2004). Spectropolarimetry was carried out for 12 type-2 QSOs and revealed polarization in all objects. Five objects show polarized broad lines expected in the framework of the unified model at the sensitivity achieved (Zakamska et al. 2005). Zakamska et al. (2006) studied the host galaxy properties for nine objects, finding that the majority (6/9) of the type-2 QSO host galaxies are ellipticals. All observations support the interpretation of the type-2 AGNs selected from the SDSS as being powerful obscured AGNs. Table 1 summarizes the sample properties.

3. OBSERVATIONS

All sources were measured in the $6_{16}-5_{23}$ line of H₂O (22.23508 GHz rest frequency). The observations were carried out during several runs at the GBT of the National Radio Astronomy Observatory (NRAO) in January and June 2005 as well as at the Effelsberg 100-m radio telescope of the Max Planck Institut für Radioastronomie (MPIfR) in November and December 2005. For details of observations, see Table 1.¹

3.1. GBT

A total of 128 SDSS type-2 AGNs were observed with the GBT, limited to those that are within the available frequency coverage of 12–15.4 GHz ($0.44 < z < 0.85$). The observing mode utilized two feeds separated by 5.5' on the sky, each with dual polarization. The system temperatures were typically 25 K. The source was placed alternately in each beam, with a position-switching interval of 2 minutes and was typically observed for 30 minutes total on-source time (possibly longer for objects with follow-ups). A total of 200 MHz

¹Note that our velocity convention is the optical one, i.e. $v = cz$.

bandwidth was covered with $\sim 0.5 \text{ km s}^{-1}$ channels. Antenna pointing checks were made roughly every 2 hours, and typical pointing errors were less than 1/10 of a full width to half power (FWHP) beamwidth of 48'' at 15 GHz. GBT flux calibration was done using standard antenna gain vs frequency curves. We estimate the calibration uncertainty to be $\sim 20\%$.

3.2. Effelsberg

A total of 150 SDSS type-2 AGNs were observed with the Effelsberg 100-m radio telescope². The measurements were carried out with a dual polarization HEMT receiver providing system temperatures of ~ 36 –45 K (for the observed frequencies between ~ 14.3 and 17.1 GHz) on a main beam brightness temperature scale. The observations were obtained in a position switching mode. Signals from individual on- and off-source positions were integrated for 3 minutes each, with the off-position offsets alternating between +900 and -900 arcsec in Right Ascension. The typical on-source integration time was ~ 70 minutes (possibly longer for objects with follow-ups) with variations due to weather and elevation. An auto-correlator backend was used, split into eight bands of 40 MHz width and 512 channels, respectively, that were individually shifted in such a way that a total of ~ 130 –240 MHz was covered. Channel spacings are $\sim 1.5 \text{ km s}^{-1}$. The FWHP beamwidth was $\sim 40''$. The pointing accuracy was better than 10''. Calibration was obtained by repeated measurements at different frequencies toward 3C 286, 3C 48, and NGC 7027, with flux densities taken from Ott et al. (1994), interpolated for the different observed frequencies using their Table 5. The calibration should be accurate to $\sim 20\%$.

4. RESULTS

All spectra were examined carefully by eye for both broad and narrow lines. In addition, we applied spectral binning using several bin sizes, especially if there was anything looking remotely like a signal.

²Note that a few objects were observed at both GBT and Effelsberg yielding a total number of 274 sources.

4.1. The Gigamaser J0804+3607

As already reported in Barvainis & Antonucci (2005), water maser emission was detected from the type-2 QSO SDSS J080430.99+360718.1 (hereafter J0804+3607; $z = 0.66$). With $L_{\text{H}_2\text{O}} \simeq 21,000 L_{\odot}$ ³, it is the intrinsically most powerful maser known.

4.2. Non Detections

While the detection of a water vapor maser in J0804+3607 shows that H₂O masers are indeed detectable at high redshift, and thus, that such a project is in principle feasible, no obvious maser emission was discovered in any of the remaining objects (Table 1). For some objects we see 2–3 sigma blips, which, however, do not meet the 5 σ detection criterion. While they are most likely statistically insignificant, considering the effectively large number of trials implicit in the number of channels per spectrum, and the number of objects observed, follow-up observations are planned for verification.

5. DISCUSSION

Ideally, we would like to estimate the detection probabilities for our sample and compare them with the (non-) detection rate.

In the local universe, water megamaser emission has been detected in about 10% of AGNs (Braatz et al. 2004). Simply extrapolating the percentage of megamasers detected in nearby Seyfert-2 galaxies to the more distant type-2 Seyferts and type-2 QSOs, leads to the expectation of finding at least ~ 27 megamasers among the 274 SDSS type-2 AGNs. However, such a naive extrapolation does not take into account the megamaser luminosity function, its evolution with redshift, the sensitivity of the survey, and intrinsic differences among the sources. We will discuss each of these issues in turn.

5.1. H₂O Maser Luminosity Function

Henkel et al. (2005a) performed a statistical analysis of 53 H₂O maser galaxies beyond the Magellanic clouds. From the maser luminosity

function (LF), i.e. the number density of objects with a given water maser luminosity per logarithmic interval in $L_{\text{H}_2\text{O}}$, they estimate that the number of detectable maser sources is almost independent of their intrinsic luminosity: The larger volume in which high luminosity masers can be detected compensates the smaller source density. This implies that masers out to cosmological distances should be detectable with current telescopes, as long as the LF is not steepening at the very high end and if suitable candidates are available. Thus, Henkel et al. (2005a) conclude that most of the detectable luminous H₂O megamasers with $L_{\text{H}_2\text{O}} > 100L_{\odot}$ have not yet been found.

We performed a similar analysis of the larger sample of masers known to date (78 sources; see Table 2) and derived a zeroth order approximation of the LF of extragalactic water maser sources. We here briefly summarize the procedure adapted from Henkel et al. (2005a); for details and a discussion of limitations, we refer the reader to Henkel et al. (2005a). To estimate the water maser LF, the standard V/V_{max} method (Schmidt 1986) was used. We divided the 78 maser sources known to date (Table 2) in luminosity bins L_b of 0.5 dex ($b = 1, \dots, 11$), covering a total range of $L_{\text{H}_2\text{O}}/L_{\odot} = 10^{-1}$ to $3 \cdot 10^4$. The differential LF value was calculated for each luminosity bin according to

$$\Phi(L_b) = \frac{4\pi}{\Omega} \sum_{i=1}^{n(L_b)} (1/V_{\text{max}})_i .$$

$n(L_b)$ is the number of galaxies with $L_b - 0.25 < \log(L_{\text{H}_2\text{O}}/L_{\odot}) \leq L_b + 0.25$ (centering on $\log(L_{\text{H}_2\text{O}}/L_{\odot}) = -0.75, -0.25, +0.25$, etc.). Following Henkel et al. (2005a), we set $\Omega = 2\pi$, approximating the sky coverage to be the entire northern sky, for the Seyfert sample. For J0804+3607, we assumed $\Omega = 0.64$ as the SDSS data release 1 from which the type-2 AGN sample of Zakamska et al. (2003) was taken covered $\sim 2100 \text{ deg}^2$. V_{max} is the maximum volume over which an individual galaxy can be detected depending on the detection limit of the survey and its maser luminosity (see also Sect. 5.2). We calculated the maser LF for three different detection limits: (a) 1 Jy km s⁻¹, (b) 0.2 Jy km s⁻¹, and (c) 0.06 Jy km s⁻¹. The first two cases are identical to the procedure in Henkel et al. (2005a), the latter case was added to include objects such as

³Using $H_0 = 75 \text{ km s}^{-1} \text{ Mpc}^{-1}$, $\Omega_{\Lambda} = 0.73$, and $\Omega_M = 0.27$. Note that the value given by Barvainis & Antonucci (2005), $L_{\text{H}_2\text{O}} = 23,000 L_{\odot}$, is higher due to a smaller value of H_0 .

the gigamaser J0804+3607⁴. From the sample of 78 sources, IC 342 is excluded in all three cases due to its too low maser luminosity. In case (a), 32 masers fall below the chosen detection limit, and in case (b), 10 galaxies were omitted. In case (c), all 77 sources are included in the LF. The resulting LFs are shown in Fig. 1.

The overall slope of the H₂O LF does not depend strongly on the chosen detection limit. Applying a linear fit to the three different LFs, we derive $\Phi \propto L_{\text{H}_2\text{O}}^{-1.4 \pm 0.1}$, comparable to Henkel et al. (2005a), but steeper than the LF for OH megamasers ($\Phi \propto L_{\text{H}_2\text{O}}^{-1.2}$) (Darling & Giovanelli 2002). The main conclusions we can draw from this new version of the water maser LF are virtually identical to those by Henkel et al. (2005a): (i) The number of sources at the upper end of the LF decays rapidly, indicating that gigamasers are intrinsically rare or that the proper sources have not yet been found — so far most surveys were focused on nearby sources. In case c, when including J0804+3607, the LF seems to raise again which is due to the much smaller area of sky covered in the survey presented here (see above). (ii) There are only a few sources in the $L_{\text{H}_2\text{O}} = 0.1 - 10 L_{\odot}$ bins. The associated slight minimum in the LF suggests that two different LFs are overlayed: one for masers in star forming regions with low luminosities ($L_{\text{H}_2\text{O}} < 0.1 - 10 L_{\odot}$) and one for maser sources in AGNs with $L_{\text{H}_2\text{O}} > 10 L_{\odot}$.

However, note that an extrapolation of the local maser LF to higher redshifts is not straightforward. It would assume no cosmological evolution, but a strong evolution of AGN activity with redshift is known. Another cautionary note we want to add is that our survey is most sensitive to narrow-line masers and that we might be missing broad-line masers. Although we binned our data in various ways to emphasize potential broad-line masers and to make them more visible, a given amount of integrated flux density would then be spread over a larger amount of noise and baseline uncertainties would become more severe. Broad lines typically arise in jet masers such as Mrk 348 (Peck et al. 2003) and NGC 1052 (Claussen et al. 1998), one exception being TXS 2226-184 where a broad maser arises from a disk maser (Ball et al.

⁴Note that for this distant object, we used the co-moving volume as maximum volume.

2005); for a discussion on jet masers see also Henkel et al. (2005b). As these broad-line masers are included in the LF of the known maser sources, we in principle introduce a systematic error when extrapolating the derived LF to our survey. However, since broad-line masers seem to be rare, we neglect this problem.

5.2. Sensitivity of the Survey

We can estimate the H₂O luminosities we would be able to detect depending on the sensitivity of our survey. Our sample lies at a redshift range of $0.3 < z < 0.83$, corresponding to luminosity distances of $D_L = 1,460 - 4,980 \text{ Mpc}^5$. The detectable H₂O luminosities depend on the sensitivity of the survey and the distance of the object (Henkel et al. 2005a). In general, it is

$$L = \frac{F_{\nu'}(\nu_0)}{1+z} \times 4\pi D_L^2 ,$$

with the specific flux $F_{\nu'}(\nu_0)$ in the observed frame. Then

$$\frac{L_{\text{H}_2\text{O}}}{L_{\odot}} = \frac{10^{-23} S_{\text{peak}}}{\text{Jy}} \times \frac{\nu_{\text{rest}}}{\text{c}} \times \frac{\Delta v}{\text{km s}^{-1}} \times \frac{1}{1+z} \\ \times 4\pi \left(\frac{3.1 \cdot 10^{24} D_L}{\text{Mpc}} \right)^2 \times \frac{1}{3.8 \cdot 10^{33}} ,$$

where $\nu_{\text{rest}} = 22.23508 \text{ GHz}$ and c the speed of light in km s^{-1} . Thus

$$\frac{L_{\text{H}_2\text{O}}}{L_{\odot}} = \left[0.023 \times \frac{S_{\text{peak}}}{\text{Jy}} \times \frac{\Delta v}{\text{km s}^{-1}} \right] \times \frac{1}{1+z} \times \left(\frac{D_L}{\text{Mpc}} \right)^2$$

(see also Solomon & Vanden Bout 2005). Assuming a characteristic linewidth of the dominant spectral feature of 20 km s^{-1} , a 5σ detection threshold of $5 \times (7.6/4.5) \text{ mJy}$ (with 7.6 mJy being the average rms of our observations for a 1 km s^{-1} channel) gives

$$\frac{L_{\text{H}_2\text{O}}}{L_{\odot}} = 0.0039 \times \frac{1}{1+z} \times \left(\frac{D_L}{\text{Mpc}} \right)^2 .$$

Thus, given the distance of our sample, we can detect H₂O luminosities of $L_{\text{H}_2\text{O}} \simeq 6,400 - 52,900 L_{\odot}$.

⁵Using $H_0 = 75 \text{ km s}^{-1} \text{ Mpc}^{-1}$, $\Omega_{\lambda} = 0.73$, and $\Omega_{\text{matter}} = 0.27$

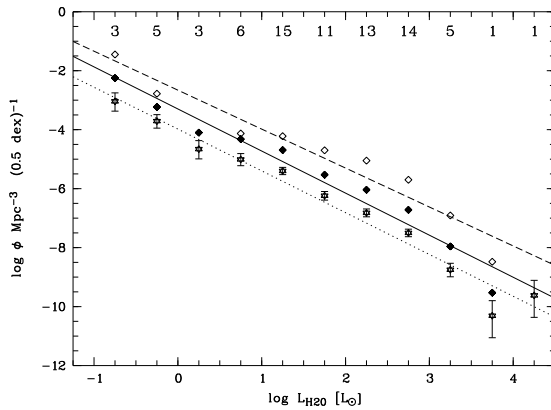


Fig. 1.— Luminosity function for water maser galaxies at $D \geq 100$ kpc (cf. Table 2). Plotted are the resulting LFs assuming three different sensitivity limits of the survey: 1 Jy km s^{-1} (open diamonds), 0.2 Jy km s^{-1} (filled diamonds), and 0.06 Jy km s^{-1} (open stars). The numbers on the top indicate the number of galaxies included in each luminosity bin for a sensitivity limit of 0.06 Jy km s^{-1} (open stars); corresponding error bars were calculated from Poisson statistics (Condon 1989). The lines indicate the best linear fit for a sensitivity limit of 1 Jy km s^{-1} (dashed line; $\Phi \propto L_{\text{H}_2\text{O}}^{-1.3}$), 0.2 Jy km s^{-1} (solid line; $\Phi \propto L_{\text{H}_2\text{O}}^{-1.4}$), and 0.06 Jy km s^{-1} , respectively (dotted line; $\Phi \propto L_{\text{H}_2\text{O}}^{-1.4}$). See text for further details.

These H_2O luminosities are higher than the average luminosity found for megamasers in Seyfert-2 galaxies and LINERs. Among the 78 known H_2O maser galaxies, the typical cumulative H_2O luminosity range is $10 \dots 2000 L_{\odot}$ for sources associated with AGNs, while most of the weaker masers appear to be related to star formation. However, in addition, there are two gigamasers known, TXS 2226–184 (Koekemoer et al. 1995) with $L_{\text{H}_2\text{O}} = 6800 L_{\odot}$ and J0804+3607 with $L_{\text{H}_2\text{O}} \simeq 21,000 L_{\odot}$. Thus, the distance of our sample allows us to detect gigamasers comparable to TXS 2226–184 and J0804+3607 only. The low detection rate may simply reflect that megamasers with H_2O luminosities above $6,000 L_{\odot}$ are intrinsically rare, an interpretation that is supported by the water maser LF (Sect. 5.1). However, there are other possibilities for the low detection rates that we discuss in the following.

5.3. Velocity Coverage

Our observations cover a frequency width of 130–240 MHz, corresponding to ~ 1800 –4000 km s^{-1} . This range should be large enough to cover any mismatch in redshift between the maser emission and the optical [OII] $\lambda 3727$ emission. For J0804+3607, for example, the megamaser line is redshifted with respect to the [OII] line by 360 km s^{-1} (Barvainis & Antonucci 2005). However, we may not be able to detect superpositions of thousands of individual maser components with slightly differing velocities nor rapidly rotating tori with only the tangential parts showing strong (highly red- and blue-shifted) maser emission (Henkel et al. 1998), if the emission covers a range of $> 2000 \text{ km s}^{-1}$.

5.4. Time Variability

Monitoring of megamaser sources has revealed variability on timescales of weeks with fluctuations of the order of 10% (e.g. Greenhill et al. 1997b) as well as on timescales of years with maser luminosities varying by factors of 3–10 (e.g. Falcke et al. 2000a; Gallimore et al. 2001; Tarchi et al. 2007). Such flaring masers can be explained by an increase in the X-ray luminosity of the AGN (Neufeld 2000), if the maser emission is powered by the X-ray radiation from the AGN.

We cannot exclude that at least some of the

sources for which we did not detect megamaser emission were in a low stage of maser activity and might be detected at a later flaring stage.

5.5. Intrinsic Differences

So far, we did not take into account that, when comparing the low-luminous AGNs such as Seyfert-2 galaxies and LINERs with the high-luminous AGNs such as the type-2 QSOs in our sample, we may be comparing apples and oranges. Intrinsic differences between the different samples complicates estimating detection probabilities.

5.5.1. The Nature of Megamaser Galaxies

So far, ~ 1500 galaxies have been searched for H₂O maser emission, resulting in the detection of 78 maser galaxies (Table 2). For 73 of the 78 known H₂O maser galaxies, the activity type has been determined (NED⁶; see Table 2). The vast majority are classified as Seyferts (78%), out of which Sy2s (including Sy1.9) are the dominant type (88%) and Sy1s are rare (3%), the rest being classified simply as Sy, or Sy1.5. The second largest activity type among the extragalactic water maser sources are LINERs, making up 11% of the sample. In addition, 7% are HII regions, 3% starburst (SB) galaxies and 1% Narrow-Line Radio Galaxies (NLRGs)⁷.

Objects with activity type of HII or SB have generally lower maser luminosities and fall in the kilomaser range ($L_{\text{H}_2\text{O}} < 10 L_{\odot}$). When including only maser sources with $L_{\text{H}_2\text{O}} \geq 10L_{\odot}$, the activity type has been determined for 57 sources in total. Out of these, 86% are Seyferts (82% are Sy2s; 4% are Sy1s, namely NGC 235A and NGC 2782), 10% are LINERs and only 2% HII regions (namely NGC 2989).

Using the higher number of extragalactic water maser sources known to date, our statistic thus confirms earlier studies that water megamaser sources are associated with AGNs of primarily Seyfert-2 or LINER type (Braatz et al. 1997, 2004). This in turn strengthens the gen-

⁶Note that NED classifications such as morphological types and activity classes are inhomogeneous.

⁷Note that we counted the “more energetic” activity type, e.g. an object with activity types “Sy2, SB, HII” (Table 2, column 10), was counted as Sy2, an object with “L, LIRG, HII”, was counted as LINER, etc.

eral expectation to find megamasers also in type-2 QSOs.

Interpreting this finding in the framework of the unified models of AGNs, where an optically thick obscuring dust torus is envisioned to encircle the accretion disk and type-1 AGNs are seen pole-on while type-2 AGNs are seen edge-on (Antonucci 1993), suggests that the megamaser activity is related to the large column densities of molecular gas along the line-of-sight in the torus. However, even if such an interpretation holds, the question remains why not all type-2 AGNs are megamasers. What are the necessary ingredients for the occurrence of these powerful masers?

Braatz et al. (1997) addressed this question by a statistical comparison of the physical, morphological, and spectroscopic properties of the known megamaser galaxies with those of non-megamaser galaxies⁸. They compared the AGN class, the host galaxy type and inclination, the mid-infrared (MIR) and FIR properties, the radio fluxes and luminosities, the [OIII] fluxes and luminosities, and the X-ray properties of the 16 megamasers known at that time with those of ~ 340 non-megamaser galaxies. Apart from their main conclusion that H₂O emission is only detected in Seyfert-2 galaxies and LINERs but not in Seyfert-1 galaxies (a conclusion that still holds for the larger sample of megamasers known today; see above), Braatz et al. (1997) found that H₂O emission is preferentially detected in sources that, when compared to the non-megamaser galaxies in their sample, are “apparently brighter at MIR and FIR and centimeter radio wavelengths”. However, this result may at least in part result from the fact that the megamaser galaxies are nearer than the non-megamaser galaxies. Braatz et al. (1997) also find that H₂O emission is preferentially detected in sources with high X-ray-absorbing columns of gas – a result that is still discussed controversially: While Zhang et al. (2006) concluded that H₂O megamasers have similar X-ray absorbing column densities as other Seyfert-2 galaxies, Greenhill et al. (2008) find a correlation between maser emission and high X-ray obscuring columns.

The requirement for velocity coherence may

⁸Here and in the following, we denote as “non-megamaser galaxies” those galaxies that have been observed at 22 GHz, but for which no megamaser emission was detected.

play an important role for the (non) occurrence of megamasers. For NGC 4258, for example, the scattered light requires a thick obscuring disk (in terms of its optical shadowing properties) but the masers reside in a thin disk (Wilkes et al. 1995; Barth et al. 1999; Humphreys et al. 2008). Enough velocity coherence (and gas column density) is perhaps achieved most often in the mid-plane. Thus, the solid angle into which the water maser emission is beamed is small, much smaller than that of the torus. With such a small angle, the likelihood to observe a maser line depending on the viewing angle is small as well.

However, now, over 10 years after the study of Braatz et al. (1997), the number of known megamaser galaxies has more than quadrupled. But there is no comparable study addressing the IR properties of megamasers, their host galaxies and their radio and optical properties. Such a study might reveal the necessary ingredients for the occurrence of megamasers in AGNs. This in turn would greatly facilitate the pre-selection of promising candidates for megamaser emission among type-2 QSOs. However, such a detailed comparison is beyond the scope of this paper.

5.5.2. FIR Luminosities and Dust Temperatures

Here, we derived the FIR luminosities and dust temperatures from IRAS fluxes (Fullmer & Lonsdale 1989) using the procedure of Wouterloot & Walmsley (1986). Some caution is required because these IRAS measurements are affected by the ratio of the contribution of nuclear light to host light which depends on nuclear FIR luminosity, nature of the host, and metric aperture size (and thus distance). Table 2 gives FIR luminosities and dust temperatures for the sample of known maser sources. The latter are all well above 30 K and thus rather large, as already noted by Henkel et al. (1986); Braatz et al. (1997); Henkel et al. (2005a).⁹ There is no obvious relation between dust temperatures and $L_{\text{H}_2\text{O}}$ (Fig. 2). In Fig. 3, we show the FIR luminosity versus water maser luminosity. There seems to be a correlation between FIR luminosity and water maser luminosities in the sense that higher FIR luminosity

⁹Note that the dust temperatures were calculated from the 60/100 μm flux ratio. Cooler dust might be dominant in these galaxies but does not radiate at these wavelengths.

lead to higher water maser luminosities. However, we do not claim that the maser luminosity versus FIR luminosity plot shows an intimate physical connection between both properties. Instead, Fig. 3 mainly shows the range of FIR and H_2O luminosities covered by the known megamaser sources.

Unfortunately, for our sample of 274 SDSS type-2 AGNs, IRAS fluxes are only available for 8 objects (see Table 3). Keeping in mind the small number statistics, it is interesting to note that the average dust temperature for these 8 objects, $T_{\text{dust,ave}} \simeq 36 \pm 1 \text{ K}$, is by $\sim 12 \text{ K}$ lower than the one for the known maser galaxies ($T_{\text{dust,ave}} \simeq 48 \pm 2 \text{ K}$). At the same time, the type-2 AGNs of the SDSS sample all have very high FIR luminosities [$\log(L_{\text{FIR}}/L_\odot) \simeq 13.5 \pm 0.1$] compared to the maser sources [$\log(L_{\text{FIR}}/L_\odot) \simeq 10.5 \pm 0.1$], which are of course a lot closer.

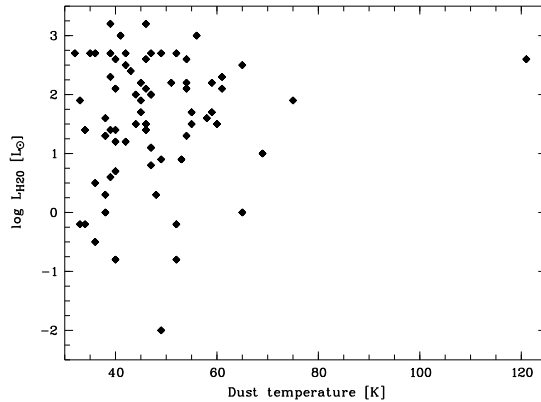


Fig. 2.— Water maser luminosities versus dust temperatures of H_2O detected galaxies (cf. Table 2; excluding those objects for which we do not have dust temperatures, leaving us with 73 objects total).

5.5.3. BH Mass and Accretion Disk

One difference between the high-z type-2 AGNs in our sample and the local Seyfert-2 galaxies and LINERs in which megamasers have been found is the mass of the central engine. For Seyfert galaxies, BH masses range between $\sim 10^6 M_\odot$ and a few $10^7 M_\odot$ (e.g. Greenhill et al. 1997b; Herrnstein et al. 1999; Henkel et al. 2002) while masses in QSOs can reach $10^9 M_\odot$ or more (e.g. Labita et al. 2006; Vestergaard et al. 2008).

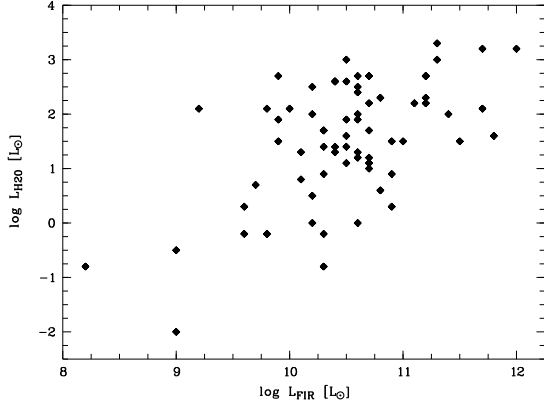


Fig. 3.— IRAS point source FIR luminosity versus total H₂O luminosity of H₂O detected galaxies (cf. Table 2; excluding those objects for which we do not have FIR luminosities as well as those for which we only have lower limits, leaving us with 71 objects total).

Tarchi et al. (2007) suggest that clouds in a disk with large rotational velocity and small galactocentric radius like NGC 4258 might not be stable in the vicinity of such a large BH mass.

5.5.4. Dust Torus and X-ray Luminosity

Barvainis & Antonucci (2005) have argued that extremely powerful masers might be expected from high-luminosity QSOs. With every square parsec of area illuminated by the primary AGN x-ray emission, a luminosity of $\sim 100 L_\odot$ is produced (Neufeld et al. 1994). The area of the torus illuminated by the AGN increases with the optical/UV continuum luminosity as the dust sublimation radius scales as $L_{\text{opt/UV}}^{1/2}$. Indeed, a scenario in which the high QSO luminosities result in gigamasers is consistent with the detection of J0804+3607, by far the most powerful maser known today. If r_{sub} increases with optical/UV luminosity, also the molecular parts giving rise to the maser emission are expected to arise further away from the nuclear engine. Such a prediction can be tested observationally: We would expect to observe rotation velocities that are smaller than in Seyfert-2 galaxies, despite a potentially more massive BH.

However, these considerations do not take into account that the dust covering factor may be decreasing with optical luminosity (Simpson 2005). In addition, the water maser luminosity is ex-

pected to grow more slowly than optical luminosity, since $L_{\text{x-ray}}/L_{\text{opt}}$ seems to be a declining function with increasing luminosity (Vignali et al. 2003). These two effects may cause megamasers to be intrinsically rare among type-2 QSOs.

5.5.5. Host Galaxy

One known difference between QSOs and Seyfert galaxies are their host galaxies: While the majority of Seyfert galaxies reside in spiral-like galaxies, QSOs are found predominantly in early-type galaxies (e.g., Disney et al. 1995; Bahcall et al. 1997; McLure et al. 1999; Floyd et al. 2004).

Among the 78 known H₂O maser galaxies, the host galaxy properties have been determined for 74 objects (NED¹⁰; see Table 2). The majority of known megamasers resides in spiral galaxies ($\sim 84\%$), of which more than half were classified as barred or at least weakly barred galaxies (53%). 7% of the host galaxies were classified as SO, and only 1% as elliptical galaxies, the rest as irregular or peculiar galaxies ($\sim 8\%$). It is remarkable that only one galaxy, namely NGC 1052, has an elliptical morphology. Also, the search for megamaser emission from early-type galaxies with FRI radio morphology lead to no detection (Henkel et al. 1998).

Does this imply that spiral galaxies somehow favor the presence of megamaser activity? Elliptical galaxies may simply lack the molecular gas necessary for the occurrence of H₂O masers. With respect to the nuclear activity, one important difference between spiral galaxies and early-type galaxies seems to be the fueling mechanism. While there is now convincing evidence that most if not all QSOs are triggered by mergers (e.g., Hutchings et al. 1994; Canalizo & Stockton 2001; Guyon, Sanders & Stockton 2006; Canalizo et al. 2007; Bennert et al. 2008; Urrutia et al. 2008), their low-luminous cousins, Seyfert galaxies, do not show unusually high rates of interaction (e.g. Malkan et al. 1998). For Seyferts, the gas necessary for the fueling of the AGN may simply be provided by their spiral host galaxies and funneled into the very center through bar instabilities

¹⁰As noted above, the morphological types given by NED are inhomogeneous.

(Combes 2006).¹¹. Bars may also play an important role for the obscuration of the central AGN (Maiolino et al. 1999). Is the fueling via bar instabilities a more stable mechanism ensuring the existence of a central dusty region in which the water molecules can survive? And are these regions destroyed by the more violent process of fueling by mergers? If this is the case, one might expect to find megamasers preferentially in barred galaxies. However, the percentage of barred galaxies in the sample of known megamasers residing in spiral galaxies is with 54% (see above) not higher than what is typically found for the fraction of barred galaxies in the local universe (e.g Barazza et al. 2008).

6. SUMMARY

We report a search for megamasers in 274 SDSS type-2 AGNs ($0.3 < z < 0.83$), half of which are luminous enough (in [OIII]) to be classified as type-2 QSOs (Zakamska et al. 2003). Apart from the detection of the gigamaser J0804+3607 already reported by Barvainis & Antonucci (2005), we do not find any additional line emission. We estimate the detection probabilities by comparing our sample with known megamasers, taking into account the observed H₂O maser luminosity function and the sensitivity of our survey. We discuss intrinsic differences between the known megamasers, mainly low-luminous AGNs such as Seyfert-2 galaxies and LINERs in the local universe, and our sample consisting of high-luminous AGNs at higher redshift. At this stage, we cannot distinguish between the different scenarios presented that could lead to the high rate of non-detections.

Further and more sensitive observations are required, e.g. using the Square Kilometer Array (SKA). Detecting megamasers in type-2 QSOs remains a challenging and yet, if successful, highly rewarding project not only to determine BH masses but especially for its possibility to constrain distances and thus the properties of the elusive dark energy.

We thank Neil Nagar for his help with the lu-

minosity function. We thank Phil Perillat and Chris Salter for help with the Arecibo observations and reductions. We thank the anonymous referee for carefully reading the manuscript and for useful suggestions. N.B. is supported through a grant from the National Science Foundation (AST 0507450). The National Radio Astronomy Observatory is a facility of the National Science Foundation operated under cooperative agreement by Associated Universities, Inc. The 100-m radio telescope at Effelsberg is operated by the Max-Planck-Institut für Radioastronomie (MPIfR) on behalf of the Max-Planck-Gesellschaft (MPG). The Arecibo Observatory is part of the National Astronomy and Ionosphere Center, which is operated by Cornell University under a cooperative agreement with the National Science Foundation. This research has made use of the NASA/IPAC Extragalactic Database (NED) which is operated by the Jet Propulsion Laboratory, California Institute of Technology, under contract with the National Aeronautics and Space Administration. For the reduction and analysis of the Effelsberg data, we used the GILDAS/CLASS software (<http://www.iram.fr/IRAMFR/GILDAS>).

REFERENCES

- Antonucci, R. R. J. 1993, *ARA&A*, 31, 473
- Argon, A. L., Greenhill, L. J., Moran, J. M., Reid, M. J., Menten, K. M., Henkel, C., Inoue, M. 1994, *ApJ*, 422, 586
- Argon, A. L. Greenhill, L. J., Moran, J. M., Reid, M. J., Menten, K. M., & Inoue, M. 2004, *ApJ* 615, 702
- Argon, A. L., Greenhill, L. J., Reid, M. J., Moran, J. M., & Humphreys, E. M. L. 2007, *ApJ*, 659, 1040
- Bahcall, J. N., Kirhakos, S., Saxe, D. H., & Schneider, D. P. 1997, *ApJ*, 479, 642
- Ball, G. H., Greenhill, L. J., Moran, J. M., Zaw, I., & Henkel, C. 2005, *ASPC*, 340, 235
- Barazza, F. D., Jogee, S., & Marinova, I. 2008, *ApJ*, 675, 1194
- Barth, A. J., Tran, H. D., Brotherton, M. S., Filippenko, A. V., Ho, L. C., van Breugel, W.,

¹¹However, the axis of the spiral disk seems to be completely uncorrelated with that of the accretion disk as traced by the radio jet (e.g. Schmitt et al. 2002).

- Antonucci, R., & Goodrich, R. W. 1999, AJ, 118, 1609
- Barvainis, R. & Antonucci, R. 2005, ApJ, 628, 89
- Baudry, A., & Brouillet, N. 1996, A&A, 316, 188
- Becker, R., Henkel, C., Wilson, T. L., & Wouterloot, J. G. A. 1993, A&A, 268, 483
- Bennert, N., Canalizo, G., Jungwiert, B., Stockton, A., Schweizer, F., Peng, C. Y., Lacy, M. 2008, ApJ, 677, 846
- Braatz, J. A., & Gugliucci, N. E. 2008, ApJ, 678, 96
- Braatz, J. A., Wilson, A. S., & Henkel, C. 1994, ApJ, 437, L99
- Braatz, J. A., Wilson, A. S., & Henkel, C. 1996, ApJS, 106, 51
- Braatz, J. A., Wilson, A. S., & Henkel, C. 1997, ApJS, 110, 321
- Braatz, J. A., Wilson, A. S., Henkel, C., Gough, R., & Sinclair, M. 2003, ApJS, 146, 249
- Braatz, J. A., Henkel, C., Greenhill, L. J., Moran, J. M., & Wilson, A. S. 2004, ApJ, 617, L29
- Braatz et al. 2007, IAUS 242, Astrophysical Masers and their Environments, eds. J. M. Chapman & W. A. Baan, Cambridge University Press, Cambridge, 399
- Brunthaler, A., Reid, M., Falcke, H., Greenhill, L. J., & Henkel, C. 2005, Sci 307, 1440
- Brunthaler, A., Henkel, C., de Blok, W. J. G., Reid, M. J., Greenhill, L. J., & Falcke, H. 2006, A&A, 457, 109
- Canalizo, G., & Stockton, A. 2001, ApJ, 555, 719
- Canalizo, G., Bennert, N., Jungwiert, B., Stockton, A., Schweizer, F., Lacy, M., & Peng, C. 2007, ApJ, 669, 801
- Castangia, P., Tarchi, A., Henkel, C. & Menten, K. M. 2008, A&A, 479, 111
- Churchwell, E., Witzel, A., Huchtmeier, W., Pauliny-Toth, I., Roland, J., & Sieber, W. 1977, A&A, 54, 969
- Claussen, M., Heiligman, G. M., & Lo, K. Y. 1984, Nature, 310, 298
- Claussen, M. J., Diamond, P. J., Braatz, J. A., Wilson, A. S., & Henkel, C. 1998, ApJ, 500, L129
- Combes, F. 2006, RMxAC, 26, 131
- Condon, J. J. 1989, ApJ, 338, 13
- Darling, J. & Giovanelli, R. 2002, ApJ, 572, 810
- Disney, M. J., et al. 1995, Nature, 376, 150
- Dos Santos, P. M., & Lépine, J. R. D. 1979, Nature, 278, 34
- Falcke, H., Henkel, C., Peck, A. B., Hagiwara, Y., Prieto, A. M., & Gallimore, J. F. 2000a, A&A, 358, L17
- Falcke, H., Wilson, A. S., Henkel, C., Brunthaler, A., & Braatz, J. A. 2000b, ApJ, 530, 13
- Floyd, D. J. E., Kukula, M. J., Dunlop, J. S., McLure, R. J., Miller, L., Percival, W. J., Baum, S. A., & O'Dea, C. P. 2004, MNRAS, 355, 196
- Fullmer, L., & Lonsdale, C. 1989, Cataloged Galaxies and Quasars Observed in the IRAS Survey, Version 2, JPL D-1932
- Gallimore, J. F., Henkel, C., Baum, S.A., Glass, I. S., Claussen, M. J., Prieto, M. A., & von Kap-Herr, S. 2001, ApJ, 556, 694
- Gardner, F. F., & Whiteoak, J. B. 1982, MNRAS, 201, 13
- Greenhill, L. J., Tilak, A., & Madejski, G. 2008, ApJL accepted (arXiv:0809.1108)
- Greenhill, L.J. 2004, New Astron. Rev. 48, 1079
- Greenhill, L. J., Herrnstein, J. R., Moran, J. M., Menten, K. M., & Velusamy, T. 1997a, ApJ, 486, L15
- Greenhill, L. J., Moran, J. M., Reid, M. J., Menten, K. M., & Hirabayashi, H. 1993, ApJ, 406, 482
- Greenhill, L. J., Jiang, D. R., Moran, J. M., Reid, M. J., Lo, K. Y., & Claussen, M. J. 1995, ApJ, 440, 619

- Greenhill, L. J., Ellingsen, S. P., Norris, R. P., Gough, R. G., Sinclair, M. W., Moran, J. M., & Mushotzky, R. 1997b, *ApJ*, 474, L103
- Greenhill, L. J., Kondratko, P. T., Lovell, J. E. J., Kuiper, T. B. H., Moran, J. M., Jauncey, D. L., & Baines, G. P. 2003a, *ApJ*, 582, L11
- Greenhill, L. J., et al. 2002, *ApJ*, 565, 836
- Greenhill, L. J., et al. 2003b, *ApJ*, 590, 162
- Guyon, O., Sanders, D. B., & Stockton, A. 2006, *ApJS*, 166, 89
- Hagiwara, Y., Diamond, P. J., & Miyoshi, M. 2002, *A&A*, 383, 65
- Hagiwara, Y., Diamond, P. J., & Miyoshi, M. 2003a, *A&A*, 400, 457
- Hagiwara, Y., Diamond, P. J., Nakai, N., & Kawabe, R. 2001a, *ApJ*, 560, 119
- Hagiwara, Y., Henkel, C., Menten, K. M., & Nakai, N. 2001b, *ApJ*, 560, L37
- Hagiwara, Y., Kohno, K., Kawabe, R., & Nakai, N. 1997, *PASJ*, 49, 171
- Hagiwara, Y., Diamond, P. J., Miyoshi, M., Rovilos, E., & Baan, W. A. 2003b, *MNRAS*, 344, L53
- Haschick, A. D., & Baan, W. A. 1985, *Nature*, 314, 144
- Henkel, C., Wouterloot, J. G. A., & Bally, J. 1986, *A&A*, 155, 193
- Henkel, C., Braatz, J. A., Greenhill, L. J., & Wilson, A. S. 2002, *A&A*, 394, L23
- Henkel, C., Tarchi, A., Menten, K. M., & Peck, A. B. 2004, *A&A*, 414, 117
- Henkel, C., Wang, Y. P., Falcke, H., Wilson, A. S., & Braatz, J. A. 1998, *A&A*, 335, 463
- Henkel, C., Güsten, R., Downes, D., Thum, C., Wilson, T. L. & Biermann, P. 1984, *A&A*, 141, L1
- Henkel, C., Peck, A. B., Tarchi, A. Nagar, N. M., Braatz, J. A., Castangia, P., & Moscadelli, L. 2005a, *A&A*, 436, 75
- Henkel, C., Braatz, J. A., Tarchi, A., Peck, A. B., Nagar, N. M., Greenhill, L. J., Wang, M. & Hagiwara, Y. 2005b, *Ap&SS* 295, 107
- Herrnstein, J. R., Moran, J. M., Greenhill, L. J., & Trott, A. S. 2005 *ApJ*, 629, 719
- Herrnstein, J. R., et al. 1999, *Nature* 400, 539
- Ho, P. T. P., Martin, R. N., Henkel, C., & Turner, J. L. 1987, *ApJ*, 320, 663
- Huchtmeier, W. K., Witzel, A., Khr, H., Pauliny-Toth, I.I., & Roland, J. 1978, *A&A*, 64, L21
- Huchtmeier, W. K., Eckart, A., & Zensus, A. J. 1988, *A&A*, 200, 26
- Humphreys, E. M. L., Reid, M. J., Greenhill, L. J., Moran, J. M., & Argon, A. L. 2008, *ApJ*, 672, 800
- Hutchings, J. B., Holtzman, J., Sparks, W. B., Morris, S. C., Hanisch, R. J., & Mo, J. 1994, *ApJ*, 429, L1
- Ishihara, Y., Nakai, N., Iyomoto, N., Makishima, K., Diamond, P., Hall, P. 2001, *PASJ*, 53, 2151
- Koekemoer, A. M., Henkel, C., Greenhill, L. J., Dey, A., van Breugel, W., Codella, C., & Antonucci, R. 1995, *Nature*, 378, 697
- Kondratko, P. T., Greenhill, L. J., & Moran, J. M., 2006, *ApJ*, 652, 136
- Kondratko, P. T., et al. 2006b, *ApJ*, 638, 100
- Labita, M., Treves, A., Falomo, R., & Uslenghi, M. 2006, *MNRAS*, 373, 551
- Lo, K. Y. 2005, *ARA&A*, 43, 625
- Malkan, M. A., Gorjian, V., & Raymond, T. 1998, *ApJS*, 117, 25
- Maiolino, R., Risaliti, G., & Salvati, M. 1999, *A&A* 341, L35
- McLure, R. J., Kukula, M. J., Dunlop, J. S., Baum, S. A., O'Dea, C. P., & Hughes, D. H. 1999, *MNRAS*, 308, 377
- Miyoshi, M., Moran, J. M., Herrnstein, J. R., Greenhill, L., Nakai, N., Diamond, P., & Inoue, M. 1995, *Nature*, 373, 127

- Morganti, R., Greenhill, L. J., Peck, A. B., Jones, D. L., & Henkel, C. 2004, New Astron. Rev. 48, 1195
- Nakai, N., Sato, N., & Yamauchi, A. 2002, PASJ, 54, L27
- Neufeld, D. A. 2000, ApJ, 542, L99
- Neufeld, D. A., Maloney, P. R., & Conger, S. 1994, ApJ, 436, L127
- Ott, M., Witzel, A., Quirrenbach, A., Krichbaum, T. P., Standke, K. J., Schalinski, C. J., & Hummel, C. A. 1994, A&A, 284, 331
- Peck, A. B., Henkel, C., Ulvestad, J. S., Brunthaler, A., Falcke, H., Elitzur, M., Menten, K. M., & Gallimore, J. F. 2003, ApJ, 590, 149
- Reid, M. J., Braatz, J. A., Condon, J. J., Greenhill, L. J., Henkel, C., & Lo, K. Y. 2008, arXiv:0811.4345v1
- Schmidt, M. 1968, ApJ, 151, 393
- Schmitt, H. R., Pringle, J. E., Clarke, C. J., Kinney, A. L. 2002, ApJ, 575, 150
- Simpson, C. 2005, MNRAS, 360, 565
- Solomon, P. M., & Vanden Bout, P. A. 2005, ARA&A, 43, 677
- Tarchi, A., Henkel, C., Chiaberge, M. & Menten, K. M. 2003, A&A, 407, L33
- Tarchi, A., Henkel, C., Peck, A. B., & Menten, K. M. 2002a, A&A, 385, 1049
- Tarchi, A., Henkel, C., Peck, A. B., & Menten, K. M. 2002b, A&A, 389, L39
- Tarchi, A., Brunthaler, A., Henkel, C., Menten, K. M., Braatz, J., & Weiß, A. 2007, A&A, 475, 497
- Tran, H. D. 2001, ApJ, 554, L19
- Trotter, A. S., Greenhill, L. J., Moran, J. M., Reid, M. J., Irwin, J. A., & Lo, K.-Y. 1998, ApJ, 495, 740
- Urrutia, T., Lacy M., & Becker, R. H. 2008, ApJ, 674, 80
- Vignali, C., Brandt, W. N., & Schneider, D. P. 2003, AJ, 125, 433
- Veron-Cetty, M.-P., & Veron, P. 1996, ESO Scientific Report, 17, 1
- Vestergaard, M., Fan, X., Tremonti, C. A., Osmor, P. S., & Richards, G. T. 2008, ApJ, 674, L1
- Wilkes, B. J., Schmidt, G. D., Smith, P. S., Mathur, S., & McLeod, K. K. 1995, ApJ, 455, 13
- Wilson, A. S., Braatz, J. A., & Henkel, C. 1995, ApJ, 455, L127
- Wouterloot, J. G. A., & Walmsley, C. M. 1986, A&A, 168, 237
- Wright, E. L. 2006, PASP, 118, 1711
- Zakamska, N. L., Strauss, M. A., Heckman, T. M., Ivezić, Z., & Krolik, J. H. 2004, AJ, 128, 1002
- Zakamska, N. L., et al. 2003, AJ, 126, 2125
- Zakamska, N. L., et al. 2005, AJ, 129, 1212
- Zakamska, N. L., et al. 2006, AJ, 132, 1496
- Zhang, J. S., Henkel, C., Kadler, M., Greenhill, L. J., Nagar, N., Wilson, A. S., & Braatz, J. A. 2006, A&A, 450, 933

TABLE 1—*Continued*

Source	z	$\log L_{\text{[OIII]}}$	FIRST	ν	rms	v range	Channel width	Telescope	Epoch
(1)	(2)	(L_{\odot})	(mJy)	(MHz)	(mJy)	(km s^{-1})	(km s^{-1})	(9)	(10)
		(3)	(4)	(5)	(6)	(7)	(8)		
231755.35+145349.4	0.311	8.10	n/a	16960.40	9.5	-1660,1600	1.4	Effelsberg	1205
231845.12-002951.4	0.397	8.00		15916.31	4.7	-500,1300	1.5	Effelsberg	1105
232902.94-002717.0	0.620	8.73		13725.40	2.1	-2180,2180	0.5	GBT	0605
232942.17+000521.2	0.446	7.89	0.97	15377.00	2.0	-1945,1945	0.5	GBT	0605
235433.86-005629.3	0.348	8.22	2.22	16494.87	6.8	-490,1240	1.4	Effelsberg	1105
235818.87-000919.5	0.402	9.32		15859.54	6.1	-500,1280	1.5	Effelsberg	1105
235831.16-002226.5	0.628	9.96		13657.90	2.2	-2195,2195	0.5	GBT	0105
235844.52-010611.9	0.684	8.53		13203.70	2.1	-2270,2270	0.5	GBT	0605

NOTE.—Col. (1): Source; bold-face: the only object for which megamaser emission was detected (Barvainis & Antonucci 2005). Col. (2): Heliocentric redshift from Zakamska et al. (2003) as measured from the [OII] $\lambda 3727$ emission line. Col. (3): Log ($L_{\text{[OIII]}}/L_{\odot}$) taken from Zakamska et al. (2003). A value of $\log (L_{\text{[OIII]}}/L_{\odot}) > 8.48$ classifies the object as a type-2 QSO. Col. (4): FIRST integrated fluxes at 20 cm in mJy taken from Zakamska et al. (2003), if the object is matched within 3''. There is no entry if the object was not detected [F_{ν} (20 cm) < 1 mJy]. "n/a" denotes those objects for which the field was not observed by the FIRST survey. Col. (5): Observed Frequency ν in MHz. Col. (6): Root mean square (rms) flux density in mJy. Col. (7): Velocity range covered by observations in km s^{-1} . Col. (8): Channel width in km s^{-1} . Col. (9): Telescope at which the source was observed. Col. (10): Date of observations (mmyy).

TABLE 2
THE 78 GALAXIES AT $D \geq 100$ KPC WITH KNOWN H₂O MASERS.

Source (1)	RA (J2000) (2)	DEC (3)	V_{syst} (km s ⁻¹) (4)	D (Mpc) (5)	$\log L_{\text{FIR}}$ (L_{\odot}) (6)	T_{dust} (K) (7)	$\log L_{\text{H}_2\text{O}}$ (L_{\odot}) (8)	Morph. (9)	Type (10)	Ref. (11)
NGC 23	00 09 53.6	+25 55 23	4566	60.9	11.1	45	2.2	SB(s)a	L,LIRG,HII	1
IC 10	00 20 27.0	+59 17 29	-350	1.2	8.2	40	-0.8	dIRR		2,3
	00 20 17.9	+59 18 31					-1.7			4
NGC 235A	00 42 52.8	-23 32 28	6519	86.9	11.4	44	2.0	S0 pec	Sy1	5
NGC 253	00 47 33.1	-25 17 17	240	3.0	10.3	52	-0.8	SAB(s)c	Sy2,SB,HII	6,7
	00 47 33.6	-25 17 14					-1.7			7
NGC 262 (Mrk 348)	00 48 47.1	+31 57 25	4505	62.0	10.4	54	2.6	SA(s)0/a:	Sy2	8,9
ESO 013-G012	01 07 00.9	-80 18 24	5045	67.0	10.7	32	2.7	Sa		10
NGC 449 (Mrk 1)	01 16 07.2	+33 05 22	4780	64.0	10.7	55	1.7	(R')S?	Sy2	11
NGC 520	01 24 34.9	+03 47 30	2281	30.4	10.9	48	0.3	Pec	SB,HII	12
NGC 598 (M 33) ^a	01 33 16.5	+30 52 53	-180	0.7	9.0	36	-0.5	SA(s)cd	HII	13,14,15,16
	01 33 28.3	+30 31 43					-1.5			15,16
	01 34 00.2	+30 40 47					-2			16,17
NGC 591 (Mrk 1157)	01 33 31.2	+35 40 06	4555	61.0	10.5	46	1.4	(R')SB0/a	Sy2	18
NGC 613	01 34 18.2	-29 25 07	1481	17.9	10.4	38	1.3	SB(rs)bc	Sy,HII	5,12
IC 0184	01 59 51.2	-06 50 25	5287	70.5	9.9 ^b	40 ^b	1.4	SB(r)a:	Sy2,HII	5
NGC 1052	02 41 04.8	-08 15 21	1470	17.0	9.2	54	2.1	E4	Sy2,L	11,20
NGC 1068	02 42 40.7	-00 00 48	1135	14.5	11.2	54	2.2	(R)SA(rs)b	Sy1,Sy2	21,22
NGC 1106	02 50 40.5	+41 40 17	4337	57.8	10.3	49	0.9	SA0+	Sy2	1
Mrk 1066	02 59 58.6	+36 49 14	3600	48.0	10.9	55	1.5	(R)SB(s)0+	Sy2	18,23
NGC 1386	03 36 46.4	-36 00 02	870	17.0	9.8	46	2.1	SB(s)0+	Sy2	24
IRAS 03355+0104	03 38 10.4	+01 14 18	11926	159.0	11.2	36	2.7 ^c	S0/a	Sy2	19
IC 342 ^d	03 46 46.3	+68 05 46	40	2.0	9.0	49	-2.0	SAB(rs)cd	Sy2,HII	25
UGC 3193	04 52 52.7	+03 03 24	4454	59.4	10.6	43	2.4	SB(rs)ab:		1
UGC 3255	05 09 50.2	+07 29 00	5675	75.0	10.6	40	1.2	SBB?	Sy2	18
Mrk 3	06 15 36.3	+71 02 15	4010	54.0	10.7	69	1.0	S0:	Sy2	18
NGC 2146	06 18 36.6	+78 21 28	900	14.5	10.9	53	0.0 ^e	SB(s)ab pec	HII	26
	06 18 38.6	+78 21 24					0.0 ^e			26
VII Zw 073	06 30 25.6	+63 40 41	11899	158.7	11.2	51	2.2		Sy2	5
NGC 2273	06 50 08.7	+60 50 45	1840	24.5	10.1	47	0.8	SB(r)a	Sy2	27
UGC 3789	07 19 30.9	+59 21 18	3325	44.3	10.2	42	2.5	(R)SA(r)ab		1
Mrk 78	07 42 41.7	+65 10 37	11195	150.0	11.0	60	1.5	SB	Sy2	18
Mrk 1210	08 04 05.8	+05 06 50	4045	54.0	10.5	75	1.9	Sa	Sy1,Sy2	11
SDSS J0804+3607	08 04 31.0	+36 07 18	$z=0.66$	3749.7 ^f	4.3 ^f		QSO2	28
2MASX J0836+3327	08 36 22.8	+33 27 39	14810	197.5	3.4 ^c		Sy2	19
NGC 2639	08 43 38.1	+50 12 20	3335	44.0	10.4	34	1.4	(R)SA(r)a:?	Sy1.9	11,29
NGC 2782	09 14 05.1	+40 06 49	2560	34.0	10.5	47	1.1	SAB(rs)a	Sy1,SB	18
NGC 2824 (Mrk 394)	09 19 02.2	+26 16 12	2760	37.0	9.9	47	2.7	S0	Sy?	30
SBS 0927+493	09 31 06.7	+49 04 47	10167	135.6	11.2	52	2.7 ^c		L ^g	19
UGC 5101	09 35 51.6	+61 21 11	11809	157.5	12.0	46	3.2	S?	Sy1.5,L,LIRG	27
NGC 2960 (Mrk 1419)	09 40 36.4	+03 34 37	4930	66.0	10.4	40	2.6	Sa?	L ^g	31
NGC 2979	09 43 08.5	-10 23 01	2720	36.0	10.0	40	2.1	(R)SA(r)a?	Sy2	30
NGC 2989	09 45 25.8	-18 22 36	4146	55.3	10.5	38	1.6	SAB(s)bc:	HII	1

TABLE 2—Continued

Source (1)	RA (2)	DEC (J2000) (3)	V_{syst} (km s $^{-1}$) (4)	D (Mpc) (5)	$\log L_{\text{FIR}}$ (L_{\odot}) (6)	T_{dust} (K) (7)	$\log L_{\text{H}_2\text{O}}$ (L_{\odot}) (8)	Morph. (9)	Type (10)	Ref. (11)
NGC 3034 (M 82)	09 55 52.2	+69 40 47	200	3.7	10.6	65	0.0	I0	SB,HII	21,32
NGC 3079	10 01 57.8	+55 40 47	1120	15.5	10.6	42	2.7	SB(s)c	Sy2,L	33,34,35
IC 2560	10 16 18.7	-33 33 50	2925	35.0	10.2	47	2.0	(R')SB(r)bc	Sy2,HII?	24,36
Mrk 34	10 34 08.6	+60 01 52	15140	205.0	11.3	56	3.0	Spiral	Sy2	23
NGC 3359	10 46 36.8	+63 13 25	1014	13.5	9.6	34	-0.2	SB(rs)c	HII	1
NGC 3393	10 48 23.4	-25 09 43	3750	50.0	10.4	46	2.6	(R')SB(s)ab	Sy2	5,27
NGC 3556	11 11 31.2	+55 40 25	700	12.0	10.2	38	0.0	SB(s)cd	HII	23
Arp 299 (Mrk 171)	11 28 32.2	+58 33 44	3120	42.0	11.7	61	2.1	IBm/SBm		23
NGC 3735	11 35 57.3	+70 32 09	2695	36.0	10.6	38	1.3	SAC	Sy2	37
NGC 4051	12 03 09.6	+44 31 53	730	10.0	9.6	38	0.3	SAB(rs)bc	Sy1.5	38
NGC 4151	12 10 32.6	+39 24 21	1000	13.5	9.8	52	-0.2	(R')SAB(rs)ab:	Sy1.5	18
NGC 4258	12 18 57.5	+47 18 14	450	7.2	9.9	33	1.9	SAB(s)bc	Sy1.9,L	21,39
NGC 4293	12 21 12.9	+18 22 57	890	17	9.7	40	0.7	(R)SB(s)0/a	L	5
NGC 4388	12 25 46.7	+12 39 44	2520	34.0	10.7	47	1.1	SA(s)b:	Sy2	18
NGC 4527	12 34 08.5	+02 39 14	1736	23.2	10.8	39	0.6	SAB(s)bc	L,HII	1
ESO 269-G012	12 56 40.7	-46 55 31	4950	66.0	10.5	41	3.0	S0	Sy2	30
NGC 4922	13 01 25.2	+29 18 50	7080	95.0	11.2	61	2.3	I0/p	Sy2,L	18
NGC 4945	13 05 27.5	-49 28 06	560	4.0	10.3	45	1.7	SB(s)cd	Sy2	40,41
NGC 5194 (M 51a)	13 29 52.7	+47 11 43	450	10.0	10.3	33	-0.2	SA(s)bc pec	Sy2,HII	6,42
NGC 5256 (Mrk 266)	13 38 17.2	+48 16 32	8365	112.0	11.5	46	1.5	Pec	Sy2,LIRG,SB	18
NGC 5347	13 53 17.8	+33 29 27	2335	31.0	9.9	44	1.5	(R')SB(rs)ab	Sy2	24
NGC 5495	14 12 23.3	-27 06 29	6589	87.8	10.8	39	2.3	(R')SA(rs)b	Sy2,HII?	5
Circinus	14 13 09.3	-65 20 21	450	4.0	10.1	54	1.3	SA(s)b:	Sy2	43,44
NGC 5506 (Mrk 1376)	14 13 14.8	-03 12 27	1850	25.0	10.3	59	1.7	SA pec	Sy1.9	11
NGC 5643	14 32 40.7	-44 10 28	1200	16.0	10.3	39	1.4	SAB(rs)c	Sy2	30
NGC 5728	14 42 23.9	-17 15 11	2795	37.0	10.6	45	1.9	(R-1)SAB(r)a	Sy2,HII	18
UGC 9618B	14 57 00.7	+24 37 03	10094	134.6	11.7	39	3.2 ^c	(Sb)	L,HII	19
NGC 5793	14 59 24.7	-16 41 36	3490	47.0	10.6	47	2.0	Sb:	Sy2	45,46
NGC 6240	16 52 58.1	+02 23 50	7340	98.0	11.8	58	1.6	I0: pec	Sy2,L	47,48,49,50
NGC 6264	16 57 16.1	+27 50 59	10177	135.7	3.1 ^c	Sb	Sy2	19
NGC 6323	17 13 18.0	+43 46 56	7790	104.0	10.3 ^h	35 ^h	2.7	Sab	Sy2	18
NGC 6300	17 17 00.3	-62 49 15	1110	15.0	10.2	36	0.5	SB(rs)b	Sy2	30
ESO 103-G035	18 38 20.3	-65 25 42	3985	53.0	10.5	121	2.6	SA0	Sy1,Sy2	24
IRAS F19370-0131	19 39 38.9	-01 24 33	6000	80.0	10.7	59	2.2	Sb	Sy2,HII	30
3C 403	19 52 15.8	+02 30 24	17690	235.0	11.3 ⁱ	...	3.3	S0	NLRG	51
NGC 6926	20 31 38.7	-80 49 58	5970	80.0	11.2	39	2.7	SB(s)bc pec	Sy2,HII	30
AM 2158-380b	22 01 17.1	-37 46 24	9661	128.8	10.4 ^h	49 ^h	2.7	Sa	Sy2,RG	5
TXS 2226-184	22 29 12.5	-18 10 47	7495	100.0	3.8	S? ^j	L	52
NGC 7479	23 04 56.7	+12 19 22	2381	31.75	10.7	42	1.2	SB(s)c	Sy2,L	1
IC 1481	23 19 25.1	+05 54 21	6120	82.0	10.6	65	2.5	S?	L	24

NOTE.—Col. (1): Source. Cols. (2,3): RA and DEC (J2000). Col. (4): Systemic velocity c z (km s^{-1}) taken from NED. Col. (5): Distance (Mpc), using $H_0 = 75 \text{ km s}^{-1} \text{ Mpc}^{-1}$. For the 53 of the 78 masers that were included in Henkel et al. (2005a), we adapt the distances from their Table 4. For a few objects, we take distances from the references listed in Col.11. Col. (6, 7): Far-Infrared (FIR) luminosity log (L_{FIR}/L_\odot) and dust temperature T_{dust} in K. For the determination of L_{FIR} and T_{dust} (60/100 μm color temperatures), see Wouterloot & Walmsley (1986). The IRAS fluxes were taken from Fullmer & Lonsdale (1989) and, for a few sources (NGC 262, NGC 598, IC 0184, NGC 4151, NGC 4258, IRAS F19370–0131, NGC 6323, 3C 403, and AM 2158–380b), from NED. Col. (8): log ($L_{\text{H}_2\text{O}}/L_\odot$), using $H_0 = 75 \text{ km s}^{-1} \text{ Mpc}^{-1}$. Col. (9) Host galaxy morphology type taken from NED. Col. (10) Activity type taken from NED (Sy = Seyfert, L = LINER, LIRG = Luminous-Infrared Galaxy, SB = Starburst, NLRG = Narrow-Line Radio Galaxy, RG = Radio Galaxy).
 Col. (11): References: [1] Braatz & Gugliucci (2008); [2] Becker et al. (1993); [3] Argon et al. (1994); [4] Henkel et al. (1986); [5] Kondratko et al. (2006b); [6] Ho et al. (1987); [7] Henkel et al. (2004); [8] Falcke et al. (2000a); [9] Peck et al. (2003); [10] Greenhill et al. (2002); [11] Braatz et al. (1994); [12] Castangia et al. (2008); [13] Churchwell et al. (1977); [14] Greenhill et al. (1993); [15] Huchtmeier et al. (1978); [16] Brunthaler et al. (2006); [17] Huchtmeier et al. (1988); [18] Braatz et al. (2004); [19] Kondratko et al. (2006a); [20] Claussen et al. (1998); [21] Claussen et al. (1984); [22] Gallimore et al. (2001); [23] Henkel et al. (2005a); [24] Braatz et al. (1996); [25] Tarchi et al. (2002a); [26] Tarchi et al. (2002b); [27] Zhang et al. (2006); [28] Barvainis & Antonucci (2005); [29] Wilson et al. (1995); [30] Greenhill et al. (2003a); [31] Henkel et al. (2002); [32] Baudry & Brouillet (1996); [33] Henkel et al. (1984); [34] Haschik & Baan (1985); [35] Trotter et al. (1998); [36] Ishihara et al. (2001); [37] Greenhill et al. (1997a); [38] Hagiwara et al. (2003b); [39] Herrnstein et al. (1999); [40] Dos Santos & Lépine (1979); [41] Greenhill et al. (1997b); [42] Hagiwara et al. (2001b); [43] Gardner & Whiteoak (1982); [44] Greenhill et al. (2003b); [45] Hagiwara et al. (1997); [46] Hagiwara et al. (2001a); [47] Hagiwara et al. (2002); [48] Nakai et al. (2002); [49] Braatz et al. (2003); [50] Hagiwara et al. (2003a); [51] Tarchi et al. (2003); [52] Koekemoer et al. (1995)

^a While the detection of two more masers has been claimed by Huchtmeier et al. (1978, 1988), we list only the three masers confirmed by Brunthaler et al. (2006).

^b L_{FIR} and T_{dust} are lower limits as there are no IRAS flux measurements at 12 and 25 μm .

^c Estimated from Fig. 1 of Kondratko et al. (2006a) using $L_{\text{H}_2\text{O}}/L_\odot = 0.023 S_{\text{total}}/(\text{Jy km s}^{-1}) \times D^2/\text{Mpc}$ with $S_{\text{total}} = \sum (1.06 S_{\text{peak}} \times \text{FWHM})$ (summed over the different components).

^d The maser luminosity refers to a brief flaring episode.

^e We assume log $L_{\text{H}_2\text{O}}/L_\odot = 0.9$ as total integrated single-dish flux density when including NGC 2146 in Figs. 1,2,3.

^f Using $H_0 = 75 \text{ km s}^{-1} \text{ Mpc}^{-1}$, $\Omega_\Lambda = 0.73$, and $\Omega_M = 0.27$.

^g Note that NED gives “Sy3” as classification, which corresponds to a LINER (Veron-Cetty & Veron 1996).

^h There is no IRAS flux measurement at 12 μm .

ⁱ There is no IRAS flux measurement at 100 μm .

^j Note that while NED lists “E/S0” as morphological classification of the host galaxy according to Koekemoer et al. (1995), Falcke et al. (2000b) favor a classification as a highly inclined spiral galaxy. We use the latter in our statistics in §5.

TABLE 3
SDSS TYPE-2 AGNs WITH IRAS FLUX MEASUREMENTS

Source (1)	z (2)	D (Mpc) (3)	$\log L_{\text{FIR}}$ (L_{\odot}) (4)	T_{dust} (K) (5)
022606.86–001656.0	0.407	2087.5	13.3	37
024919.01–000722.5	0.579	3193.5	13.7	37
031319.96+003715.6	0.395	2014.6	13.3	38
032240.60+001626.0	0.344	1711.3	13.1	35
075238.68+390304.9	0.654	3707.8	13.8	37
110709.36+511328.6	0.441	2297.4	13.5	32
123453.10+640510.2	0.594	3294.9	13.9	37
172603.09+602115.7	0.333	1647.4	13.1	35

NOTE.—Col. (1): Source. Col. (2): Heliocentric redshift from Zakamska et al. (2003) as measured from the [OII] $\lambda 3727$ emission line. Col. (3): Distance (Mpc), using $H_0 = 75 \text{ km s}^{-1} \text{ Mpc}^{-1}$, $\Omega_\Lambda = 0.73$, and $\Omega_M = 0.27$. Col. (4, 5): FIR luminosity $\log (L_{\text{FIR}}/L_{\odot})$ and dust temperature T_{dust} in K (see also Table 2 and text for details).

A. ADDITIONAL OBSERVATIONS

In addition to the SDSS type-2 AGNs, a sample of 76 radio galaxies at $z = 0.3\text{--}0.7$ was observed during the same observing runs at the GBT and the Effelsberg 100-m radio telescope (Table 4). An additional sample of high-redshift radio galaxies was observed at Arecibo Observatory (see A1; Table 4). The radio galaxies were selected from objects in NED classified as “galaxy” and “radio source” whose frequencies were accessible to the different telescope receivers and whose declinations were in the observatory range. Also, a few sources classified as galaxy or QSO were observed (26 in total; Table 5).

A.1. Arecibo

A total of 71 objects with $z = 1.1\text{--}3.6$ were observed during observing runs in October 2003, June and September 2004, and March 2005 in dual polarization, single beam, position-switching mode (see Table 4). Each observation consisted of typically 5 on/off scans of 10 minutes each, resulting in a total duration of 50 minutes per source. (However, some objects only have 2 or 3 individual scans.) Total spectrometer bandwidths of either 25 MHz or 50 MHz were divided into 1024 channels. Antenna gain, as determined from previous measurements by Arecibo staff, ranged from about 3 K/Jy to 7 K/Jy, depending on frequency, and flux calibration was done using these values obtained from a lookup table. We estimate that calibrations are accurate to 20%. Pointing was checked approximately every two hours using extragalactic radio sources.

TABLE 4—Continued

Source (1)	RA (2)	DEC (J2000) (3)	z (4)	ν (MHz) (5)	rms (mJy) (6)	v range (km s $^{-1}$) (7)	Channel width (km s $^{-1}$) (8)	Telescope (9)	Epoch (10)
87GB 180705.8+683108	18 06 50.1	+68 31 43	0.580	14072.80	2.0	-2130,2130	0.5	GBT	0605
4C +68.20	18 15 24.8	+68 06 32	0.230	18077.00	18.4	-1540,1490	1.3	Effelsberg	1205
87GB 182301.2+660210	18 23 02.8	+66 03 25	0.370	16230.00	12.9	-1660,1740	1.4	Effelsberg	1205
3C 379.1	18 24 33.0	+74 20 59	0.256	17703.00	26.1	-1580,1530	1.3	Effelsberg	1205
87GB 182631.5+651051	18 26 41.7	+65 12 43	0.646	13508.60	2.1	-2215,2215	0.5	GBT	0605
87GB 183438.3+620153	18 35 10.9	+62 04 08	0.519	14634.10	1.9	-2045,2045	0.5	GBT	0605
87GB 200332.8+661716	20 03 54.5	+66 25 56	0.456	15271.40	2.0	-1960,1960	0.5	GBT	0605
PKS2008-068	20 11 14.2	-06 44 04	0.547	14386.50	2.1	-2080,2080	0.5	GBT	0605
3C 410	20 20 06.5	+29 42 14	0.249	17809.00	23.1	-1580,1540	1.3	Effelsberg	1205
4C +02.51	20 36 34.8	+02 56 54	2.130	7103.83	1.1	-590,250	2.0	Arecibo	0904
PMN J2037-0010	20 37 13.4	-00 10 59	1.512	8851.51	7.2	-844,844	1.6	Arecibo	0904
B2 2050+36	20 52 52.1	+36 35 35	0.354	16422.00	13.3	-1680,1710	1.4	Effelsberg	1205
2MASX J20580405-0018416	20 58 04.1	-00 18 42	0.336	16643.00	16.2	-1630,1700	1.4	Effelsberg	1205
PMN J2058+0542	20 58 28.8	+05 42 51	1.381	9338.51	4.3	-800,800	1.5	Arecibo	0904
3C 427.1	21 04 06.4	+76 33 12	0.572	14158.10	1.9	-2115,2115	0.5	GBT	0605
4C +23.56	21 07 14.8	+23 31 45	2.483	6383.86	1.3	-1080,320	2.2	Arecibo	0904
4C +03.49	21 09 21.8	+03 26 52	1.634	8441.53	2.9	-890,890	1.7	Arecibo	0904
87GB 211905.7+182558	21 21 25.5	+18 39 09	1.861	7771.75	1.0	-930,930	1.9	Arecibo	0904
3C 434	21 23 16.3	+15 48 06	0.322	16819.00	26.5	-1670,1620	1.4	Effelsberg	1205
3C 435	21 29 06.1	+07 33 06	0.471	15115.60	1.4	-1980,1980	0.5	GBT	0605
4C +19.71	21 44 07.5	+19 29 15	3.594	4840.00	1.0	-1550,1550	1.0	Arecibo	1003
3C 436	21 44 11.7	+28 10 18	0.215	18308.00	24.3	-1540,1480	1.3	Effelsberg	1205
3C 437	21 47 25.1	+15 20 37	1.480	8965.73	2.9	-835,835	1.6	Arecibo	1003
4C +26.59	21 58 25.4	+26 52 37	0.713	12980.20	1.6	-2310,2310	0.6	GBT	0605
MRC 2202+128	22 05 14.3	+13 05 32	2.706	5999.73	1.1	-1250,1250	2.4	Arecibo	1003
TXS 2226+162	22 28 43.9	+16 33 16	1.519	8826.91	2.9	-850,850	1.6	Arecibo	1003
4C +11.68	22 29 57.5	+11 27 36	0.238	17960.00	18.3	-1570,1510	1.3	Effelsberg	1205
4C -04.85	22 39 32.8	-04 29 34	0.552	14340.20	1.4	-2090,2090	0.5	GBT	0605
TXS 2252+186	22 54 53.7	+18 57 02	2.153	7052.01	0.9	-510,1020	2.0	Arecibo	0904
PKS 2305+033	23 08 25.1	+03 37 04	2.457	6431.87	0.9	-560,1170	2.2	Arecibo	0904
PMN J2320+0500	23 20 44.7	+04 59 30	0.635	13599.40	2.2	-2204,2204	0.5	GBT	0605
87GB 231912.7+222125	23 21 42.2	+22 37 52	2.553	6258.09	0.8	-1200,1200	2.3	Arecibo	0904
MRC 2332+154	23 34 58.4	+15 45 50	2.480	6389.36	0.7	-1120,0	2.2	Arecibo	0904
3C 467	23 48 29.6	+18 44 05	0.632	13624.40	2.1	-2200,2200	0.5	GBT	0605
4C +10.74	23 51 26.9	+10 34 54	1.334	9526.56	2.5	-785,785	1.6	Arecibo	1003
4C +28.58	23 51 59.2	+29 10 29	2.891	5714.47	1.0	-1310,1310	2.5	Arecibo	1003

NOTE.—Col. (1): Source. Col. (2,3): Right ascension and declination (J2000) taken from NED. Col. (4): Heliocentric redshift z taken from NED. Col. (5): Observed Frequency ν in MHz. Col. (6): rms flux density in mJy. Col. (7): Velocity range covered by observations in km s $^{-1}$. Col. (8): Channel width in km s $^{-1}$. Col. (9): Telescope at which the source was observed. Col. (10): Date of observations (mmyy).

TABLE 5
DETAILS OF OBSERVATIONS: MISCELLANEOUS SOURCES

Source	Classification	RA	DEC	z	ν	rms	v range	Channel width	Telescope	Epoch
(1)	(2)	(3)	(4)	(5)	(MHz)	(mJy)	(km s $^{-1}$)	(km s $^{-1}$)	(10)	(11)
		(J2000)			(6)	(7)	(8)	(9)		
081404.54+060238.3	QSO	08 14 04.5	+06 02 38	0.561	14235.00	2.3	-2105,2105	0.5	GBT	0605
082110.76+031758.4	QSO	08 21 10.8	+03 17 58	0.451	15324.00	3.3	-1955,1955	0.5	GBT	0605
083134.21+290239.5	G	08 31 34.2	+29 02 40	0.568	14180.50	1.5	-2110,2110	0.5	GBT	0605
091345.49+405628.2	G	09 13 45.5	+40 56 28	0.442	15430.30	2.2	-1940,1940	0.5	GBT	0605
092344.07+081051.2	QSO	09 23 44.1	+08 10 51	0.415	15703.00	12.7	-1730,1780	1.5	Effelsberg	1205
093737.11+370535.4	G	09 37 37.1	+37 05 35	0.449	15334.60	2.2	-1955,1955	0.5	GBT	0605
095005.83+481338.6	G	09 50 05.8	+48 13 39	0.375	16171.00	11.9	-1680,1730	1.4	Effelsberg	1205
095019.90+051140.9	G	09 50 19.9	+05 11 41	0.523	14590.00	2.0	-2055,2055	0.5	GBT	0605
100258.68+050812.0	G	10 02 58.7	+05 08 12	0.512	14705.70	2.0	-2035,2035	0.5	GBT	0605
101401.59+431543.4	G	10 14 01.6	+43 15 43	0.511	14715.50	2.0	-2035,2035	0.5	GBT	0605
102853.93+514323.1	G	10 28 53.9	+51 43 23	0.417	15681.00	11.3	-1710,1800	1.5	Effelsberg	1205
103822.07+523115.9	QSO	10 38 22.1	+52 31 16	0.598	13914.30	2.1	-2150,2150	0.5	GBT	0605
112907.10+575605.4	G	11 29 07.1	+57 56 05	0.312	16935.00	10.0	-1660,1600	1.4	Effelsberg	1205
113710.78+573158.8	G	11 37 10.8	+57 31 59	0.395	15939.00	7.5	-1690,1750	1.5	Effelsberg	1205
2MASS J12324114+1112587	G	12 32 41.1	+11 12 59	0.249	17802.31	1.3	-500,1100	1.3	Effelsberg	1105
134021.43+564319.3	QSO	13 40 21.4	+56 43 19	0.572	14144.50	1.9	-2115,2115	0.5	GBT	0605
141318.96+415658.8	G	14 13 19.0	+41 56 59	0.533	14504.30	2.1	-2065,2065	0.5	GBT	0605
141918.90+510240.2	G	14 19 18.9	+51 02 40	0.324	16794.00	26.0	-1680,1620	1.4	Effelsberg	1205
142939.80+395935.3	G	14 29 39.8	+39 59 35	0.531	14523.20	2.0	-2060,2060	0.5	GBT	0605
143017.34+521735.1	QSO	14 30 17.4	+52 17 35	0.367	16254.00	12.2	-1680,1720	1.4	Effelsberg	1205
153944.13+343503.9	QSO	15 39 44.1	+34 35 04	0.551	14336.00	2.0	-2090,2090	0.5	GBT	0605
155143.91+434758.1	G	15 51 43.9	+43 47 58	0.618	13733.90	1.7	-2180,2180	0.5	GBT	0605
161401.64+380807.5	G	16 14 01.6	+38 08 08	0.350	16470.00	13.4	-1630,1700	1.4	Effelsberg	1205
162459.70+332253.4	QSO	16 24 59.7	+33 22 53	0.504	14784.00	1.4	-2025,2025	0.5	GBT	0605
163653.37+245746.4	QSO	16 36 53.4	+24 57 46	0.584	14028.50	1.5	-2135,2135	0.5	GBT	0605
164424.58+344636.9	QSO	16 44 24.6	+34 46 37	0.587	14010.80	1.6	-2135,2135	0.5	GBT	0605

NOTE.—Col. (1): Source. Col. (2): Classification as Galaxy (G) or QSO, taken from NED. Col. (3,4): Right ascension and declination (J2000) taken from NED. Col. (5): Heliocentric redshift z taken from NED. Col. (6): Observed Frequency ν in MHz. Col. (7): rms flux density in mJy. Col. (8): Velocity range covered by observations in km s $^{-1}$. Col. (9): Channel width in km s $^{-1}$. Col. (10): Telescope at which the source was observed. Col. (11): Date of observations (mmyy).